Journal of Nanoparticle Research (2006) 8:971–980
DOI 10.1007/s11051-006-9094-5

Size determination of Au aerosol nanoparticles by off-line TEM/STEM observations

Lisa S. Karlsson[1,*], Knut Deppert[2] and Jan-Olle Malm[1]
[1]*Materials Chemistry, P.O. Box 124, Lund, SE-22100, Sweden;* [2]*Solid State Physics, P.O. Box 118, Lund, SE-22100, Sweden; *Author for correspondence (Tel.: +46-46-2228232; Fax: +46-46-2224012; E-mail: lisa.karlsson@materialkemi.lth.se)*

Received 17 June 2005; accepted in revised form 22 February 2006

Key words: aerosol, nanoparticles, size determination, image analysis, measurements, TEM, STEM

Abstract

Determination of particle size distributions of Au aerosol nanoparticles has been performed by a TEM/STEM investigation. The particles are generated by an evaporation/condensation method and are size-selected by differential mobility analyzers (DMA) based on their electrical mobility. Off-line TEM measurements resulted in equivalent projected area diameters assuming that the particles are spherical in shape. In this paper critical factors such as magnification calibration, sampling, image analysis, beam exposure and, particle shape are treated. The study shows that the measures of central tendency; mean, median and mode, are equal as expected from a narrow size distribution. Moreover, the correlation between TEM/STEM and DMA are good, in practice 1:1. Also, STEM has the advantage over TEM due to enhanced contrast and is proposed as an alternative route for determination of particle size distributions of nanoparticles with lower contrast.

Introduction

Aerosol particles with nanometer dimensions attain great interest as potential candidates for applications where controls over particle parameters are important issues (Kruis et al., 1998). Particle diameter is a critical measure and the aerosol community has developed a number of devices to control or determine particle size. The most pronounced one being the Differential Mobility Analyzer (DMA). In its various appearances from the first report (Knutson & Whitby, 1975) via the Nano-DMA (Chen et al., 1998) to the newest development (Flagan, 2004) it allows classification of aerosol particles according to their electrical mobility (Z). However, the corresponding electrical mobility diameter (D_p) is an indirect measure of size and is only equivalent to the geometric diameter for particles of spherical shape. Transmission electron microscopy (TEM) on the other hand is an excellent mean to determine particle area equivalent diameters and particle shape and is being extensively used for this purpose. However, the full method for particle size determination is seldom described and control of common sources of error (National Institute of Standards and Technology, 2001) is not always possible. In the nanoparticle size regime, where TEM is one of a few possible techniques, reliable and objective size measuring routines are necessary to avoid biased characterization (Fisker et al., 2000; Reetz et al., 2000; Weibel et al., 2005).

For aerosol nanoparticles the combination of DMA and TEM is a powerful tool in understanding the properties of different systems. We have designed and tested a method for statistical

image sampling and equivalent area diameter determination by TEM for aerosol nanoparticles. Here, we report on the diameter determination of size-selected Au aerosol nanoparticles by off-line TEM and scanning transmission electron microscopy (STEM). Critical issues to consider in determination of particle size distributions with TEM/STEM are; magnification calibration, sampling statistics, image analysis criteria, beam exposure and, particle shape and these are treated in this paper.

Experimental

Aerosol nanoparticles were produced in a standard tandem DMA set-up as described earlier by Magnusson et al. (1999). Au metal was placed in a ceramic boat in a furnace heated to 1850°C to ensure formation of Au vapour. The sheath gas (ultra-pure N_2) transported the vapour out of the furnace. Cooling of the vapour resulted in formation of fractal-like agglomerates of primary particles (Karlsson et al., 2005). The agglomerates were then charged by a ^{63}Ni radioactive β emitting 'neutralizer' and size selected in a first DMA. Compaction of the size selected agglomerates was performed in a second furnace set at 600°C. A second DMA was used to select the desired size fraction of the compacted aerosol nanoparticles. The concentration of the final size-selected aerosol was determined by an electrometer based on the fact that the majority of the particles were singly charged (Wiedensohler, 1988). Depositions of the aerosol nanoparticles onto lacey carbon film Cu TEM grids were done in a deposition chamber by applying a perpendicular electric field. The resulting concentration of particles on the lacey carbon film was 10–15 particles/ μm^2.

Both of the DMAs in the set-up were of the home-built Vienna type (Winklmayr et al., 1991), i.e., a cylindrical DMA with a central electrode rod in a coaxial tube electrode. The radial dimensions of the inner central rod (r_1) and the outer tube (r_2) electrodes being 25 and 33 mm, respectively. A laminar sheath gas flow (Q_{sh}) of ultra-pure N_2 is kept constant through the DMA along the central rod. The aerosol flow (Q_a) enters the DMA through a slit, with a width of 1 mm, in the outer annulus next to the outer tube electrode. An outlet slit for the selected size fraction is situated at the opposite end of the DMA next to the central rod. The tube electrode is grounded and the voltage (U) of the central rod electrode can be varied between 0–6500 and 0–3500 V for the first and the second DMA, respectively. The classification length (L), from the aerosol inlet to the outlet, of the DMAs was 110 mm. In order for an aerosol nanoparticle to be size selected the radial and axial travel times must be equal. This means that the mean electrical mobility (Z_p^*) of the size selected particles can be expressed as in Eq. (1) if symmetrical flows are assumed (Knutson & Whitby, 1975).

$$Z_p^* = \frac{Q_{sh} \ln (r_2/r_1)}{2\pi UL} \tag{1}$$

The corresponding electrical mobility diameter (D_p) depends on the electrical mobility (Z_p) as given in Eq. 2.

$$D_p = \frac{n_e C_c}{3\pi\eta Z_p} \tag{2}$$

Here, n_e is the number of electron charges (e) on the particle; C_c is the Cunningham factor and η the viscosity of the gas. The Cunningham factor (Eq. 3) adjusts for slip due to non-zero velocity of the surrounding gas at the particle surface. C_c depends on the size of the particle and increases with reduced particle diameter, the factor is most pronounced when the particle diameter approached the mean free path (λ) of the surrounding gas.

$$C_c = 1 + \frac{\lambda}{D_p}\left[2.34 + 1.05\exp\left(-0.39\frac{D_p}{\lambda}\right)\right] \tag{3}$$

The relative full width of the electrical mobility range, $\Delta Z_p/Z_p^*$ will depend on the ratio of the aerosol flow, Q_a and the sheath flow, Q_{sh} (Eq. 4).

$$\frac{\Delta Z_p}{Z_p^*} = 2\frac{Q_a}{Q_{sh}} \tag{4}$$

In the ideal case this gives a symmetric triangular transfer function. However, diffusion will affect the trajectories of the particles and effectively broaden the transfer function (Flagan, 1999). Other factors influencing the transfer function are non-symmetric or non-laminar flows and unwanted electrical fields. In this study Q_a was set to 1.68 l min^{-1} and Q_{sh} was 10 l min^{-1}, i.e., the flow ratio was 1/6. Thus, the width of the aerosol size

distribution was $\pm 1/6\ D_p$ if diffusion broadening is neglected.

The instrument used for TEM/STEM image acquisition was a 300 kV FEG-TEM (JEOL 3000-F FEG TEM) with 0.16 nm point resolution in conventional TEM (CTEM) mode and 0.13 nm in high-angle annular dark field (HAADF)-STEM mode. Images were recorded with a 2k×2k CCD camera in CTEM, i.e., 2048×2048 pixels and with a semiconductor detector with digital out-put in STEM (chosen image size, 1024 × 1024 pixels). The calibration of the TEM was made intrinsically by acquiring high resolution images of the particles using known crystallographic distances as reference. Fourier transforms of the HRTEM images were used to identify the orientation of the particle, hence single distances could be identified. The ratio between the measured distances and distances reported in literature (Lihl et al., 1971) was within a range of 1.00 ± 0.03. The calibration of magnifications used was also checked by comparing the resulting area of a specific particle at two magnification settings, one with atomic resolution and one at lower magnification to be used for the particle analysis. This comparison showed an accuracy of $\pm 5\%$ between the magnifications in conventional mode. As the deviations were symmetric around 1:1 correlation in both the absolute and the magnification table calibration the accuracy of calibrations was considered to be acceptable. Hence, data could be collected by acquiring low magnification images complemented with high resolution reference images at certain intervals, e.g., every 5th image. This resulted in a large amount of measured particles but with a minimum amount of images. The low magnification images were taken of neighbouring areas, without overlap, on the lacey carbon film in a stepwise manner. In this way the images were taken without operator bias towards particles with a preferential position and/or orientation, a common problem when viewing one particle at a time. The low magnification was chosen so that the pixel size was 0.5 nm or smaller in conventional mode to reduce any systematic errors due to lack of resolution in the image, e.g., for a spherical particle of 15 nm in diameter one pixel corresponds to 1.4‰ of its cross-sectional area at 0.5 nm/pixel. In total, for this study, six different samples were investigated by CTEM, one of them was also studied in bright field (BF)-STEM and HAADF-STEM modes to investigate the potential of these methods. STEM has the capacity of higher (BF) or inverse (HAADF) amplitude contrast as compared to conventional TEM due to the choice of direct or scattered electrons, respectively (Williams & Carter, 1996, p. 352).

The samples studied were prepared at three different occasions; batch i–iii. The depositions were made during daily routine runs of particle production and the size was varied within 10–50 nm. The off-line measurements of individual aerosol nanoparticles have been made from the acquired CTEM and STEM images with the image analysis software Semper 6 Plus (Synoptics Ltd., Cambridge, England). A particle analysis program routine was written in this software to analyse properties such as area (A) and circularity (C) (Eq. 5, p is the perimeter) based on the amplitude contrast of the particles in the images.

$$C = \frac{4\pi A}{p^2} \tag{5}$$

Before analysis the images were converted from the acquisition software Digital Micrograph 3.7.0 to Semper 6 Plus. To facilitate the image analysis X-ray hits were removed and CTEM image size was reduced to 1200 × 1200 pixels. X-ray hits normally generate single bright pixels that will affect the grey level settings. The reduced image size simply limited the size of the Semper files to avoid unnecessary long computation times. However, this reduction would increase the pixel size by a factor of 2.9, i.e., the area of one pixel will after the reduction correspond to 4.2‰ of the cross sectional area of a spherical particle 15 nm in diameter. The selection of the particle cross-sectional areas was made by adjusting the parameters of an intensity transformation table overlaying the image of interest. The table was directly related to the original image with respect to its grey levels. By a semi-automatic adjustment of the upper and lower limits of the grey levels in the table a selection could be implemented. When the selected range agreed with the particle cross-section in the original image, the range was accepted. An example of such a selection is given in Figure 1, showing the original CTEM image, the selected particles and a correlation of the two. Touching particles could be separated manually by defining the interface between them (indicated by arrows in

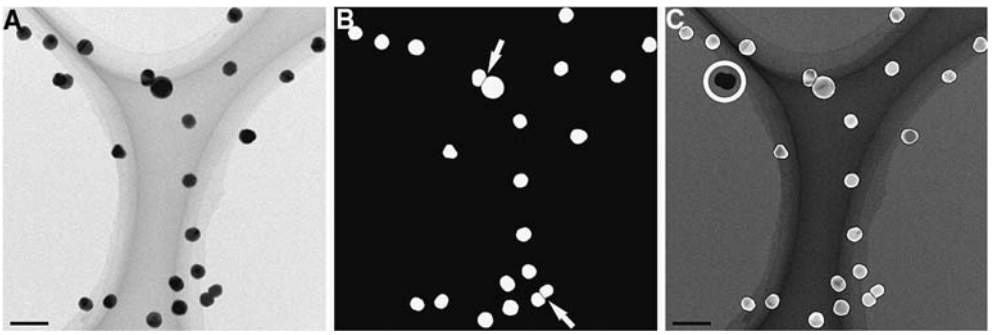

Figure 1. Defining particles in Semper 6 Plus. (A) A typical CTEM image of sample IV. (B) Selection of particles based on their contrast. Separation performed for touching particles as indicated by the arrows, overlapping particles are disregarded. (C) A comparison of CTEM (A) and the particle selection (B) by overlap of the images. Disregarded particles are encircled. The scale bar corresponds to 100 nm in each image.

Figure 1B). For overlapping particles only visible outlines could be defined. If the outlines were indistinguishable none of the overlapping particles were included in the selection (encircled in Figure 1C). Even missing parts due to partial selection could be accounted for by filling and defining the rim of the particle manually. Partial selection mainly occurred when the contrast of the carbon film was high, due to thickness, and the selection range was chosen in order to minimize any contributions from the carbon film. Once the selection was made the particle cross-sections could be analysed. Extreme cases could be omitted from the selection by defining a maximum and minimum cross-sectional area of interest. In this way artefacts such as single pixels, high contrast areas and overlapping particles could be eliminated. The parameters used in this study were cross-sectional area (A) and circularity (C).

Results and discussions

Although TEM/STEM images are 2D-projections, a random orientation of the nanoparticles on the supporting lacey carbon film should circumvent the possibility of any systematic error in measured size. Since the deposition of the nanoparticles is accomplished by electrostatic precipitation from the random aerosol phase (Krinke et al., 2002) it is reasonable to assume that the orientation is in fact random on the lacey carbon film. Overlap of particles on the substrate occurs on occasion, specifically at higher deposition concentrations. As only separable particles were included in the selection, with the particle analysis program, broadening of the particle size distribution due to overlap are omitted in this investigation.

The electron beam exposure during the TEM investigation implies interactions between the electrons and the Au. An investigation by Rez and Glaisher (1991) showed that the energy deposited into single Au nanoparticles >15 nm is not sufficient for melting or rotation to occur. The dominating interaction process is knock-on damage where single atoms are displaced in the structure. This does not dramatically change the overall morphology of the nanoparticles. As the samples where transported in ambient air when transferred from the aerosol generator to the TEM, condensation of water and, oxidation formation are possible contamination sources. However, in the vacuum of the TEM column (10^{-5} Pa) water is prone to evaporate. Also, Au is known for its high reduction potential and only has one known oxide forming at alkaline conditions (Greenwood & Earnshaw, 2002). We therefore conclude that the measured area largely corresponds to the *in situ* state of the nanoparticles.

Typical TEM and STEM images are shown in Figure 2 with the enhanced contrast visible for the HAADF-STEM-image. The obtained particle area from the analysis program was used to calculate the equivalent cross-sectional area diameter, d_A assuming that the particles are spherical. The resulting particle size distributions of the CTEM investigation for the six different samples (I–VI) with D_p 15, 20, 34, 40, 44 and 50 nm, respectively are presented as histograms in Figure 3 and the corresponding averages and standard deviations

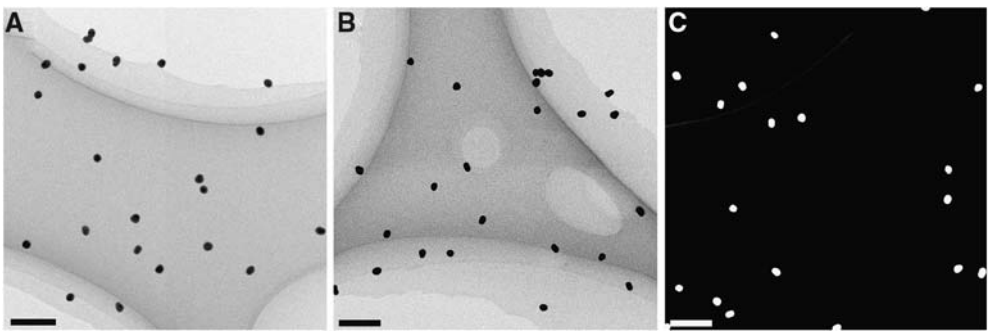

Figure 2. Typical low magnification images of sample II in CTEM (A), BF-STEM (B) and HAADF-STEM (C). The scale bar in each image corresponds to 100 nm. The HAADF-STEM image was acquired with 0.8 nm probe size and camera length set to 51–134 mrad.

are given in Table 1. The size distributions are close to normal in appearance with a minor peak at larger diameters for all samples. The normal appearance is supported by the fact that the mean ($\bar{d}_A$), median (d'_A) and mode ($\hat{d}_A$) values lie within $\pm 4\%$ for each sample. A minor peak occurs at about 1.5 times $\hat{d}_A$ of the major peak. For the size range of these samples, a doubly charged particle with the equivalent D_p would have a geometric diameter of 1.43–1.45 times the geometric diameter of a singly charged particle. Thus, the minor peak observed in the histograms is most likely an effect of doubly charged particles being selected by the DMA.

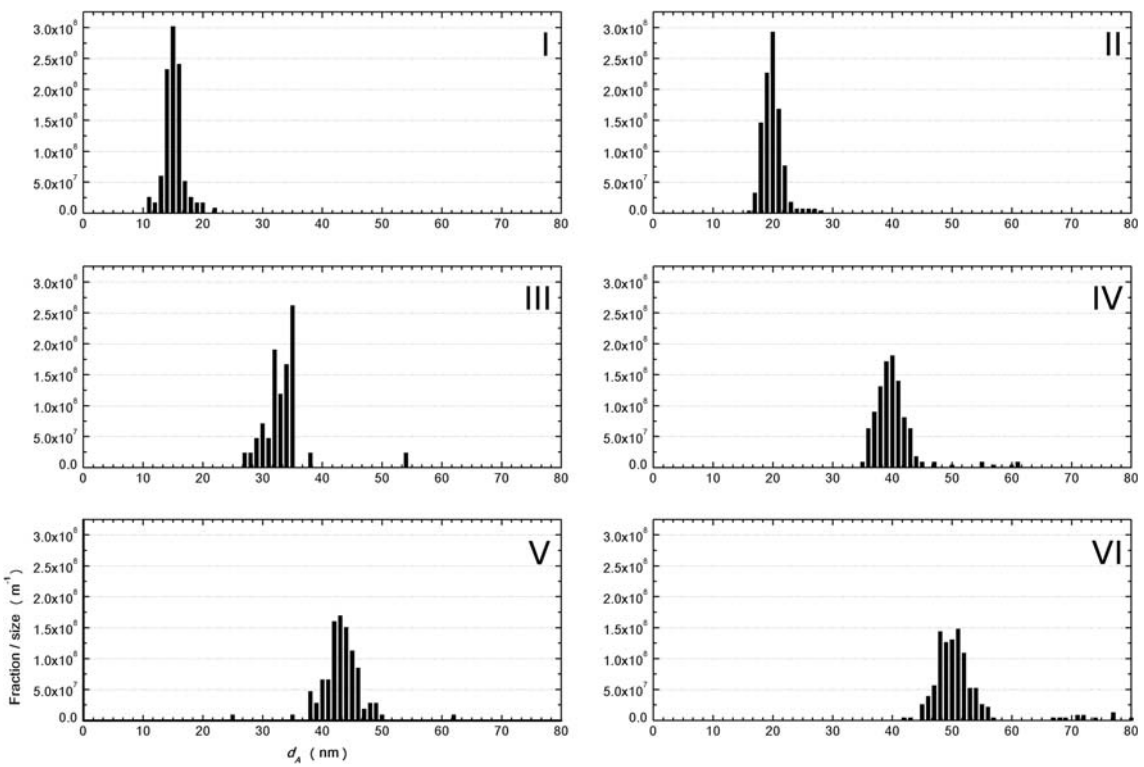

Figure 3. Histograms of particle size distributions from CTEM investigation of samples I–VI. The axis labels are equal in all cases and are given by the bottom left graph. The height of the histograms is standardized with respect to size interval (Δd_A) and total counts and is expressed as fraction of the total number of particles per unit of size interval (number/m).

Table 1. Measures of central tendency (median (d'_A), mean ($đ_A$), and mode ($\hat{d}_A$)) and variability (standard deviation (σ)) of the particle size distributions from CTEM and STEM analysis for the samples I–VI. BF and DF indicate BF-STEM and HAADF-STEM, respectively; when nothing else is stated CTEM was used

Sample	Batch	# Particles	D_p[a] (nm)	d'_A[b] (nm)	$đ_A$[c] (nm)	σ	$\hat{d}_A$[d] (nm)
I	ii	116	15	14.49	14.62	1.70	15.61
II	iii	273	20	19.22	19.42	1.71	19.11
II-BF	iii	278	20	19.25	19.44	1.86	19.97
II-DF	iii	97	20	19.52	19.84	2.42	19.78
III	i	42	34	32.83	32.84	4.01	n.a.
IV	iii	221	40	39.16	39.69	3.80	38.14
V	i	106	44	42.71	42.73	3.71	44.11
VI	iii	229	50	49.77	50.79	5.77	49.46

[a]FWHM of DMA; [b]d'_A, median; [c]$đ_A$, mean; [d] $\hat{d}_A$, mode.

When comparing the results of the DMA and CTEM, respectively (Figure 4) it is evident that D_p is corresponding well to all three measures of central tendency. Linear fitting shows that the relation with D_p follows the order $\hat{d}_A < d'_A < đ_A$ with slopes of 0.981, 0.994 and 0.998, respectively and the intercept close to origo in all three cases. The standard deviations (σ) increase with D_p as expected and stays within $\pm 1/6$ of D_p as calculated from the flow ratio of the DMA (Eq. 4) with diffusion broadening neglected. Both d'_A and $đ_A$ are sensitive to out-liers, $đ_A$ more so than d'_A, in the distribution and can be affected by any bias in the histograms, e.g., the minor peak. The bimodality is not accounted for by the DMA as both particle modes are equivalent when it comes to Z. If the doubly charged fraction is large the bias will be greater and both d'_A and $đ_A$ will be shifted towards larger sizes. Clearly this will result in deviations when comparing with D_p. However, this investigation shows that median (d'_A), mean ($đ_A$), and mode ($\hat{d}_A$) all give rather accurate measures of the electrical mobility equivalent diameter, D_p when bias is low. This means that if the distributions are suffering from bias, the mode value can be used for correlation. This was done by Park et al. (2004) when studying fractal like agglomerates of soot from the exhaust of a diesel engine. Although, the

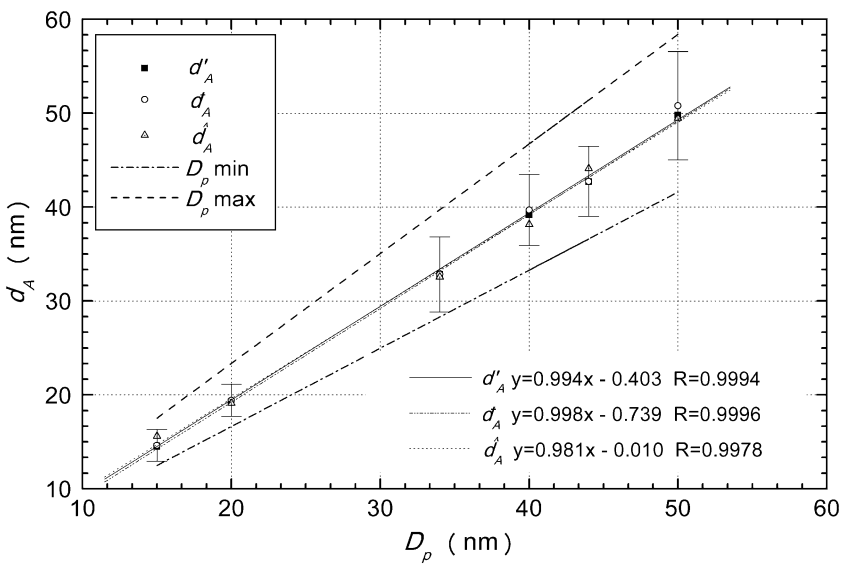

Figure 4. Comparison of different measures of central tendency (median (d'_A), mean ($đ_A$), and mode ($\hat{d}_A$)) of the particle size distributions given in the histograms of Figure 3. The range of possible D_p:s from the DMA, as determined from Eq. 4, is given by the minimum (dash-dot) and maximum (dash) limits. Results of linear fitting are also included.

aerosol suffered from fragmentation and doubly charged agglomerates causing up to three different size modes the correlation between CTEM and DMA was on average only 2% off by overestimation from the DMA. The comparison, between the methods, was made using the mode of the projected area equivalent diameter ($D_{\text{projected}}$) measured by CTEM and the peaks of the expected size distribution of the DMA.

Deviations in particle size between DMA and TEM have otherwise been reported extensively earlier, both by ourselves and others, with a common deviation of 10–15% overestimation by the DMA. Without precautions, such as intrinsic calibration, it is in fact common to have this discrepancy as the absolute calibration of the TEM is set for a given condition (Williams & Carter, 1996, p. 148). Our first study (Hummes et al., 1996) was made by atomic force microscopy (AFM) to determine the transfer function of the DMA. There we concluded a good agreement between the shape of the transfer function and the measured size distribution for sintered Ag particles, however, with overestimation of the diameter by the DMA. Other off-line characterizations with TEM confirmed the overestimation of the diameter of aerosol nanoparticles by the DMA of GaAs by approximately 50% (Deppert et al., 1996), Ag by approximately 32% (Hummes et al., 1996) and Au and Ag aerosol nanoparticles by 10 and 5%, respectively (Karlsson et al., 2004). However, for AuGa core-shell aerosol nanoparticles an underestimation of 2% has been measured (Karlsson et al., 2004). In all of the TEM investigations the mean diameter ($\bar{d}$) was used for comparison with D_p. It should be noted that changes in methodology such as statistical image sampling and internal calibration have now brought us from 10% overestimation by the DMA to 1:1 correlation for Au aerosol nanoparticles. This clearly highlights the necessity of an accurate methodology.

Kuga et al. (2001) reported 15% overestimation in D_p by a low pressure DMA as compared to the count mean Feret diameter, $\bar{d}_{\text{F}}$ determined by TEM for Ag and CsI nanoparticles. Nasibulin et al. (2001) reported 15% overestimation of the geometric mean diameter, $\bar{d}_{\text{g}}$ by a DMA/CPC system for Cu/CuO nanoparticles in comparison with TEM. Close to 1:1 correlations have also been noted between DMA and TEM as e.g., Camata et al. (1996) with a radial DMA for Si nanoparticles up to 10 nm. A slight (2%) underestimation of D_p as compared to the count mean diameter ($\bar{d}_p$) was obtained by TEM. Many of these investigations do not explicitly report on how the TEM was calibrated or if an internal calibration was used. On the other hand high resolution TEM (HRTEM) is often mentioned as a mean to determine the crystalline phase of the material studied, which would indicate the possibility to perform an internal calibration. A solution to the calibration issue may be the use of standard samples of known diameter and shape for calibration of DMA and TEM, respectively. This has been reported by Mulholland et al. (1999), in which case the resulting correlation for a third sample of 100 nm spherical polystyrene particles was 1:1 after the calibration.

Sample II was also analysed with STEM BF (II-BF) and HAADF (II-DF), the resulting histograms and data are given in Figure 5 and Table 1, respectively. As is evident from the histograms the correlation between CTEM, BF-STEM and HAADF-STEM is very good for sample II. Both the median (d'_A) and the mean ($\bar{d}_A$) diameters correlate well between the methods, especially for CTEM and BF (Table 1). It has been reported by Walther (2004) that CTEM and HAADF-STEM correlates well for 7 nm Co crystals but that CTEM overestimates the size for 2 nm Pt crystals. The contrast in CTEM is decreasing with the size of the crystals and therefore the detectability is affected. In our case the diameter is 15 nm or above and it is reasonable to expect a good correlation between the methods. It should also be noted that the particle definition step is greatly facilitated by the use of HAADF-STEM images as the contrast is enhanced. The good correlation between HAADF-STEM and CTEM is promising for analysis of materials of lower contrast.

The circularity of the particles (Figure 6A) divides the samples into two regimes (I, III & V and II, IV & VI) almost corresponding to the different batches from the aerosol generator. The purity of the samples was checked by X-ray energy dispersive spectroscopy (XEDS) resulting in no detectable presence of impurities. Hence, we believe that the differing circularity is probably an effect of different batches and the conditions of the aerosol generator set-up. The correlation of the circularity between the different methods

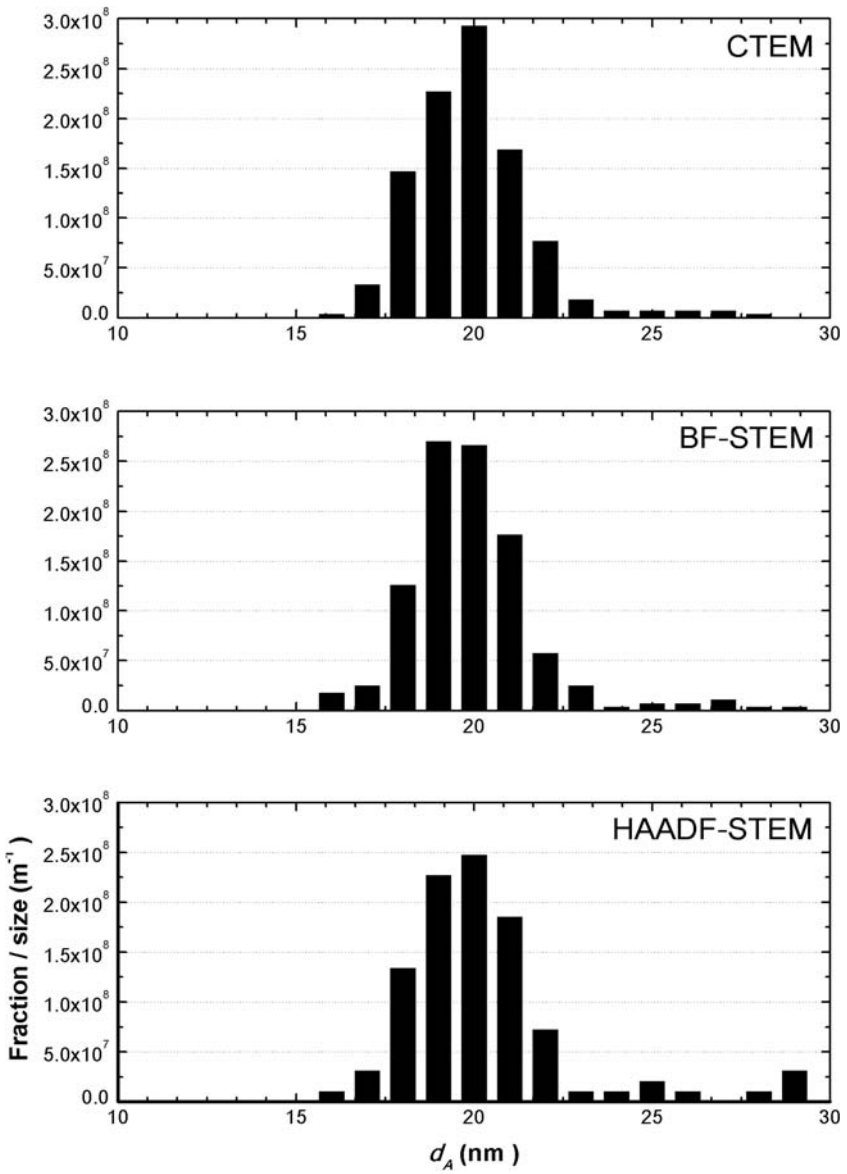

Figure 5. Histograms of particle size distributions of sample II based on investigation method; CTEM, BF-STEM and HAADF-STEM, respectively. The axis labels are equal in all cases and are given by the bottom graph. The height of the histograms is standardized with respect to size interval (Δd_A) and total counts and is expressed as fraction of the total number of particles per unit of size interval (number/m).

(Figure 6B) shows good agreement for CTEM and HAADF-STEM. However, the BF-STEM analysis shows a levelling above circularity of 0.9. As the sample is identical this is most likely an artefact of the method.

In this investigation we focused on the reliability of DMAs in daily use, with regular cleaning of the DMAs. This means that gradual deposition of particles onto the electrodes of the DMAs will occur. The particle deposition will decrease r_2/r_1 as the flow region of the aerosol and sheath gas is reduced. This results in a decrease in Z_p^* (Eq. 1) and subsequently an increase of D_p. Hence, in comparison with the original settings of a clean

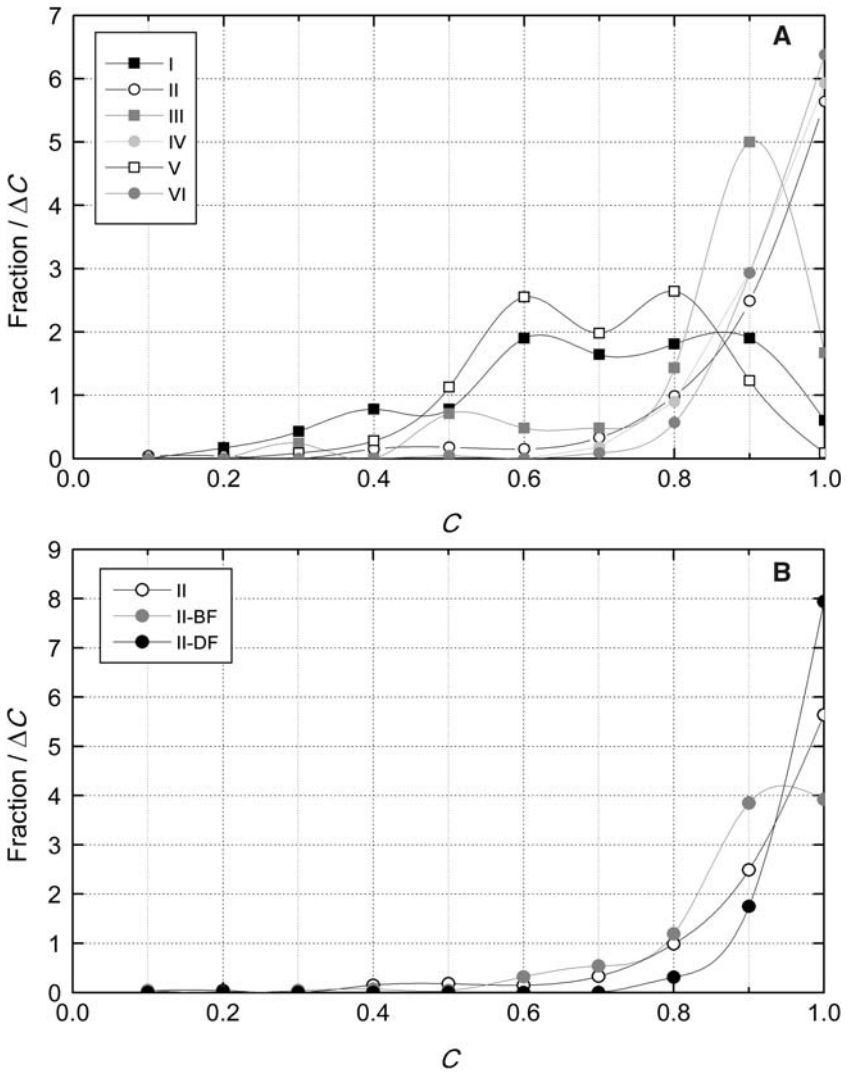

Figure 6. Circularity of particles in samples I–VI (A) as determined from CTEM and sample II (B) from BF-STEM and HAADF-STEM, respectively. Circularity (C) of 1 equals a perfect sphere. The height is standardized with respect to circularity interval (ΔC) and total counts.

DMA the deposition will result in a shift of the transfer function towards larger D_p, i.e., the original setting underestimates D_p. To our knowledge there is no study reported in literature on the effects of gradual deposition onto the electrodes and the corresponding transfer function. However, regular cleaning at low levels of deposition build-up should circumvent this effect. In this study we see little effect on different batches except for in circularity of the particles. Thus, we conclude that the reliability of a routinely operated DMA is good.

Conclusions

A method for determining particle size distributions with TEM/STEM has been designed and evaluated with promising results. Critical concepts to consider are internal magnification calibration and statistical image sampling. Both BF- and HAADF-STEM investigations agree to a high degree with the results of CTEM and are proposed as an alternative route for particle size distribution determination of lower contrast particles. It is also noted that the reliability of a routinely operated

DMA is good, with only differences in circularity being observed between three different batches.

Acknowledgements

This work was performed within the Nanometer Structure Consortium at Lund University and supported by the Swedish Research Council (VR) and the Swedish Foundation for Strategic Research (SSF). Martin N. A. Karlsson and Brent A. Wacaser are kindly acknowledged for producing the Au aerosol nanoparticle samples. Anna Carlsson is kindly acknowledged for supplying the particle analysis program routine.

References

Camata R.P., H.A. Atwater, K.J. Vahala & R.C. Flagan, 1996. Size classification of silicon nanocrystals. Appl. Phys. Lett. 68, 3162–3164.

Chen D.-R., D.Y.H. Pui, D. Hummes, H. Fissan, F.R. Quant & G.J. Sem, 1998. Design and evaluation of a nanometer aerosol differential mobility analyzer (Nano-DMA). J. Aerosol Sci. 29, 497–509.

Deppert K., J.-O. Bovin, J.-O. Malm & L. Samuelson, 1996. A new method to fabricate size-selected compound semiconductor nanocrystals: Aerotaxy. J. Crystal Growth 169, 13–19.

Fisker R., J.M. Carstensen, M.F. Hansen, F. Bødker & S. Mørup, 2000. Estimation of nanoparticle size distributions by image analysis. J. Nanopart. Res. 2, 267–277.

Flagan R.C., 1999. On differential mobility analyzer resolution. Aerosol Sci. Technol. 30, 556–570.

Flagan R.C., 2004. Opposed migration aerosol classifier (OMAC). Aerosol Sci. Technol. 38, 890–899.

Greenwood N.N. & A. Earnshaw, 2002. Chemistry of the Elements 2nd edn. Oxford: Butterworth-Heinemann 1181.

Hummes D., S. Neumann, F. Schmidt, M. Drötboom, H. Fissan, K. Deppert, T. Junno, J.-O. Malm & L. Samuelson, 1996. Determination of the size distribution of nanometer-sized particles, Europ. Aerosol Conf., Delft, The Netherlands. J. Aerosol Sci. 27, S163–S164.

Karlsson L.S., K. Deppert, M.N.A. Karlsson & J.-O. Malm, 2004. Proceedings of the 13th European microscopy congress Vol II (Materials Science), Belgian Society of Microscopy. Belgium: Antwerp pp. 107–108.

Karlsson M.N.A., K. Deppert, L.S. Karlsson, M.H. Magnusson, J.-O. Malm & N. Srinivasan, 2005. Compaction of agglomerates of aerosol nanoparticles: A compilation of experimental data. J. Nanopart. Res. 7, 43–49.

Knutson E.O. & K.T. Whitby, 1975. Aerosol classification by electric mobility: Apparatus, theory, and applications. J. Aerosol Sci. 6, 443–451.

Krinke T.J., K. Deppert, M.H. Magnusson, F. Schmidt & H. Fissan, 2002. Microscopic aspects of the deposition of nanoparticles from the gas phase. J. Aerosol Sci. 33, 1341–1359.

Kruis F.E., H. Fissan & A. Peled, 1998. Synthesis of nanoparticles in the gas phase for electronic, optical and magnetic applications – a review. J. Aerosol Sci. 29, 511–535.

Kuga Y., K. Okauchi, D. Takeda, Y. Ohira & K. Ando, 2001. Classification performance of a low pressure differential mobility analyzer for nanometer-sized particles. J. Nanopart. Res. 3, 175–183.

Lihl F., H. Ebel & W. Baumgartner, 1971. Röntgenographische Untersuchungen zur Vegardschen Regel. Zeitschrift für Metallkunde 62, 42–45.

Magnusson M.H., K. Deppert, J.-O. Malm, J.-O. Bovin & L. Samuelson, 1999. Gold nanoparticles: Production, reshaping, and thermal charging. J. Nanopart. Res. 1, 243–251.

Mulholland G.W., N.P. Bryner & C. Croarkin, 1999. Measurement of the 100 nm NIST SRM 1963 by differential mobility analysis. Aerosol Sci. Technol. 31, 39–55.

Nasibulin A.G., E.I. Kauppinen, D.P. Brown & J.K. Jokiniemi, 2001. Nanoparticle formation via copper (II) acetylacetonate vapour decomposition in the presence of hydrogen and water. J. Phys. Chem. B 105, 11067–11075.

National Institute of Standards and Technology., 2001. NIST Recommended Practice Guide Special Publication 960–1: Particle Size Characterization. Washington: US Government Printing Office 85.

Park K., D.B. Kittelson & P.H. McMurry, 2004. Structural properties of diesel exhaust particles measured by transmission electron microscopy (TEM): Relationships to particle mass and mobility. Aerosol Sci. Technol. 38, 881–889.

Reetz M.T., M. Maase, T. Schilling & B. Tesche, 2000. Computer image processing of transmission electron micrograph pictures as a fast and reliable tool to analyze the size of nanoparticles. J. Phys. Chem. B 104, 8779–8781.

Rez P. & R.W. Glaisher, 1991. Measurement of energy deposition in transmission electron microscopy. Ultramicroscopy 35, 65–69.

Walther T., 2004 Proceedings of the 13th European microscopy congress Vol II (Materials Science), Belgian Society of Microscopy. Belgium: Antwerp 119–120.

Weibel A., R. Bouchet, F. Boulc'h & P. Knauth, 2005. The big poblem of small particles: A comparison of methods for determination of particle size in nanocrystalline anatase powders. Chem. Mater. 17, 2378–2385.

Wiedensohler A., 1988. An approximation of the bi-polar charge distribution for particles in the submicron size range. J. Aerosol Sci. 19, 387–389.

Williams B.D. & C.B. Carter, 1996. Transmission Electron Microscopy. New York: Plenum Press p. 352 and p.148.

Winklmayr W., G.P. Reischl, A.O. Lindner & A. Berner, 1991. A new electromobility spectrometer for the measurement of aerosol size distributions in the size range from 1 to 1000 nm. J. Aerosol Sci. 22, 289–296.